Journal of Exposure Science & Environmental Epidemiology
https://doi.org/10.1038/s41370-018-0102-5

ARTICLE

Metabolomic assessment of exposure to near-highway ultrafine particles

Douglas I. Walker[1,2,8] · Kevin J. Lane[3] · Ken Liu[1] · Karan Uppal[1] · Allison P. Patton[4] · John L. Durant[2] · Dean P. Jones[1] · Doug Brugge[2,5,6] · Kurt D. Pennell[2,7]

Received: 10 January 2018 / Revised: 6 September 2018 / Accepted: 12 November 2018

Abstract

Exposure to traffic-related air pollutants has been associated with increased risk of adverse cardiopulmonary outcomes and mortality; however, the biochemical pathways linking exposure to disease are not known. To delineate biological response mechanisms associated with exposure to near-highway ultrafine particles (UFP), we used untargeted high-resolution metabolomics to profile plasma from 59 participants enrolled in the Community Assessment of Freeway Exposure and Health (CAFEH) study. Metabolic variations associated with UFP exposure were assessed using a cross-sectional study design based upon low (mean 16,000 particles/cm^3) and high (mean 24,000 particles/cm^3) annual average UFP exposures. In comparing quantified metabolites, we identified five metabolites that were differentially expressed between low and high exposures, including arginine, aspartic acid, glutamine, cystine and methionine sulfoxide. Analysis of the metabolome identified 316 *m/z* features associated with UFP, which were consistent with increased lipid peroxidation, endogenous inhibitors of nitric oxide and vehicle exhaust exposure biomarkers. Network correlation analysis and metabolic pathway enrichment identified 38 pathways and included variations related to inflammation, endothelial function and mitochondrial bioenergetics. Taken together, these results suggest UFP exposure is associated with a complex series of metabolic variations related to antioxidant pathways, in vivo generation of reactive oxygen species and processes critical to endothelial function.

Keywords Exposome · High-resolution metabolomics · Metabolome-wide association study · Traffic-related air pollution

Introduction

Particulate air pollution is a key environmental risk factor for human health, with global disease burden estimates suggesting 3.1 million deaths in 2010 were attributable to ambient particulate exposure [1]. A recent analysis of >60 million Medicare beneficiaries showed a 7.3% increase in all-cause mortality for every increase of 10 μg/m^3 in fine particle matter ($PM_{2.5}$, particulate matter with diameter ≤ 2.5 μm) [2]. Acute exposure to pollutants from traffic-related sources has been shown to be associated with changes in systemic inflammation, DNA methylation, gene expression, and respiratory function [3–6]; however, underlying toxicological mechanisms are not known.

The metabolome, which includes all low molecular weight (<2000 dalton) chemical species present in biological matrices, is a functional measure of the interaction between the genome, diet, environment, and the

Supplementary material The online version of this article (https://doi.org/10.1038/s41370-018-0102-5) contains supplementary material, which is available to authorized users.

✉ Kurt D. Pennell
kurt_pennell@brown.edu

1 Clinical Biomarkers Laboratory, Division of Pulmonary, Allergy, Critical Care and Sleep Medicine, School of Medicine, Emory University, Atlanta, GA, USA

2 Department of Civil and Environmental Engineering, Tufts University, Medford, MA, USA

3 Department of Environmental Health, Boston University School of Public Health, Boston, MA, USA

4 Health Effects Institute, Boston, MA, USA

5 Department of Public Health and Community Medicine, Tufts University School of Medicine, Boston, MA, USA

6 Jonathan M. Tisch College of Civic Life, Tufts University, Medford, MA, USA

7 School of Engineering, Brown University, Providence, RI, USA

8 Present address: Department of Environmental Medicine and Public Health, Icahn School of Medicine at Mount Sinai, New York, NY, USA

Published online: 05 December 2018

biochemical processes required for life [7]. Identifying the metabolic changes associated with environmental exposures can provide insight into the mechanisms underlying exposure-related diseases. Untargeted metabolomic techniques based upon ultra-high resolution mass spectrometry now make possible measurement of up to 20,000 chemical features, providing sufficient characterization for precision medicine and exposome research [8].

Limited study of the metabolomic effects of air pollution suggest metabolic response to is detectable on both short-term and long-term exposure timescales; however, variations unique to acute and chronic exposure have not been established. In the study by Breitner, Schneider et al. [9], $PM_{2.5}$ and ozone exposure were estimated based upon residential address (10-km grid) for participants in a cardiac catheterization cohort. Metabolomic measures included 61 metabolites, related to amino acid metabolism, fatty acid metabolism and total ketones, with only 10 used to assess association with $PM_{2.5}$ and ozone. The results suggested a delayed association with decreased arginine and glycine based upon previous day $PM_{2.5}$ levels. Other metabolomic studies of traffic-related pollution include a multi-platform assessment of lavage fluids following chamber exposures to biodiesel exhaust [10], 5-h ambient pedestrian exposure [11] and occupational exposure of office workers, traffic cops and rickshaw drivers in India [12]. Only one study has examined the relationship between long-term $PM_{2.5}$ exposure and metabolic changes. Menni, Metrustry et al. [13] showed significant metabolic variations associated with residential $PM_{2.5}$ exposure that included four amino acid-related metabolites, benzoate, glycerate and the antioxidant α-tocopherol, in a subset of the TwinsUK cohort. These metabolites were also linked to a decline in lung function within a larger cohort from this study, suggesting a protective role for α-tocopherol. While these studies provided insight into metabolic variations associated with air pollution exposure, limitations included minimal metabolome coverage and lack of individualized exposure levels and primarily represented acute exposures only.

In the present study, we performed high-resolution metabolomics (HRM) of plasma collected from participants enrolled in the Community Assessment of Freeway Exposure and Health (CAFEH) study to assess metabolic variations associated with exposure to ultrafine particles (UFP, <0.1 μm). We first evaluated central metabolic intermediates that were quantified using reference standardization, which was followed by a metabolome-wide association study (MWAS) to identify systemic variations in metabolism associated with UFP exposure. We then utilized the metabolic correlation structure and pathway enrichment for insight into the relationship between exposure, biological response and disease pathobiology.

Methods

Study population

A subset of 59 participants from the CAFEH study was selected for HRM profiling. CAFEH is a community-based participatory research study of the relationship between traffic-related air pollution and health effects in individuals living in the Boston area (MA, USA). Details of the study population and design can be found elsewhere [14, 15]. Briefly, recruitment occurred in near- (≤500 m from major highways) and far- (≥1000 m) highway areas. Participants were recruited based upon age (≥40 years) and a geographically-weighted, random selection process. Blood samples were collected by visiting a clinic during normal business hours from August 2009 to June 2010; the majority of samples were collected in winter, spring and fall. All participants provided informed consent and the study was approved by the Tufts University School of Medicine Institutional Review Board. For this metabolomics study, participant selection criteria included non-smokers and individuals with documented low (mean 16,000 particles/cm ^{3}) or high (mean 24,000 particles/cm^3) UFP exposure and was restricted to non-Hispanic white residents of Somerville and Dorchester/South Boston.

Exposure assessment

The methodology for predicting individual time-activity adjusted (TAA) UFP exposure levels has been described previously [14, 16, 17]. Hourly ambient particle number concentration (PNC), a proxy for UFP, was first estimated at fine spatial resolution (20 m) using predictive multivariable regression models [16]. PNC measurements were obtained with a condensation particle counter (TSI Model 3775; particle size 4–3000 nm) in each study area by driving a mobile monitoring lab along fixed routes at various times of the day, on all days of the week and in all seasons (35–47 days per study area) over the course of one year [18].

Individualized annual average PNC were obtained by adjusting hourly ambient PNC estimates to correct for time spent in different microenvironments over a year-long period [19]. We first averaged the ambient PNC values predicted by the model for all hours of the year ($n = 8760$ h) to calculate a residential average ambient (RAA) PNC for each residence. To derive TAA-PNC, we used hourly questionnaire data for five micro-environments (inside home, outside home, at work, on highway, and other)

and we accounted separately for PNC infiltration into the home. The time-activity information was used to assign time spent inside or outside home, at work/school, and at other locations for each hour of the day. Participants provided weekly window opening information from December to February (winter) and June to August (summer). Participants also reported air conditioner type and usage. We assigned the residential-PNC value to all hours spent inside the home, assuming 100% particle infiltration. This assumption was based upon previously published analyses of homes in our study population that showed a 0.95 median indoor–outdoor ratio [20]. For those with work-based TRAP exposure, we approximated exposures by using the average hourly RAA-PNC of all participants residing ≤50 m of a major highway for the hours they were at work. For participants without TRAP exposure at work, we approximated their work PNC exposures using the average hourly RAA-PNC of all participants residing in the urban background area. For time spent in all other micro-environments, we also assigned the hourly residential average of all participants residing in the urban background area based on the assumption that urban background was the most likely exposure for any micro-environment in the metropolitan area.

High-resolution metabolomics

HRM was completed using established methods by an analyst blinded to sample identity [21]. Briefly, plasma samples were prepared and analyzed in batches of 20; each batch included duplicate analysis of pooled human plasma (QStd-3) for reference standardization. Prior to analysis, plasma aliquots were removed from storage at −80 °C and thawed on ice. A 65 µL aliquot of plasma was then treated with 130 µL of LC-MS grade acetonitrile, equilibrated for 30 min on ice and centrifuged (16.1 × *g* at 4 °C) for 10 min to remove precipitated proteins. The supernatant was added to an autosampler vial and maintained at 4 °C until analysis.

Sample extracts were analyzed using liquid chromatography (LC) and Fourier transform high-resolution mass spectrometry (Dionex Ultimate 3000, Q-Exactive HF, Thermo Scientific). For each sample, 10 µL aliquots were analyzed in triplicate using hydrophilic interaction liquid chromatography (HILIC) with electrospray ionization (ESI) source operated in positive mode and reverse phase chromatography (RPC) with ESI operated in negative mode. This use of complementary chromatography phases and ionization polarity has been shown to improve detection of endogenous and exogenous chemicals [22]. Analyte separation was accomplished by HILIC using a 2.1 mm × 100 mm × 2.6 µm Accucore HILIC column (Thermo Scientific) and an eluent gradient (A = 2% formic acid, B = water, C = acetonitrile) consisting of an initial 1.5 min period of 10% A, 10% B, 80% C, followed by linear increase to 10% A, 80% B, 10% C at 6 min and then held for an additional 4 min, resulting in a total runtime of 10 min per injection. Reverse phase separation was by 2.1 mm × 100 mm × 2.6 µm Accucore C_{18} column (Thermo Scientific) using an eluent gradient consisting of an initial 2 min period of 0.5% A, 94.5% B, 5% C, followed by a linear increase to 0.5% A, 4.5% B, 95% C at 6 min and held for the remaining 4 min. For both methods, mobile phase flow rate was held at 0.35 mL/min for the first 1.5 min, increased to 0.5 mL/min and held for the final 4 min.

The high-resolution mass spectrometer was operated in full scan mode at 120,000 resolution and mass-to-charge ratio (*m/z*) range 85–1275. Probe temperature, capillary temperature, sweep gas and S-Lens RF levels were maintained at 200 °C, 300 °C, 1 arbitrary units (AU), and 45 AU, respectively, for both polarities. Positive tune settings for sheath gas, auxiliary gas, sweep gas and spray voltage setting were 45 AU, 25 AU, and 3.5 kV, respectively; negative settings were 30 AU, 5 AU and −3.0 KV. Raw data files were extracted and aligned using apLCMS [23] with modifications by xMSanalyzer[24]. Uniquely detected ions consisted of accurate mass *m/z*, retention time and ion abundance, referred to as *m/z* features. Prior to data analysis, *m/z* features were batch corrected using ComBat [25] and filtered to remove those with coefficient of variation (CV) ≥ 75% or greater than 20% non-detected values in both groups.

Reference standardization

To determine concentrations of metabolites critical to metabolic homeostasis and clinical health markers, 79 metabolites previously confirmed by comparison to authentic reference standards were quantified by reference standardization [26]. Using this approach, metabolite concentrations were first determined in Q-Std3 by methods of addition or comparison to NIST standard reference material 1950 (Metabolites in Frozen Human Plasma) [27–29], providing a reference standard for each analyte. Plasma concentrations were calculated using single point calibration by multiplying the analyte response factor (calculated as the ratio between the known concentration of the compound being quantified and ion intensity in Q-Std3 or NIST 1950) and metabolite intensity detected in each study sample. Metabolite concentrations were compared to previously reported values in the human metabolome database (HMDB) [7] and data from the National Health and Nutrition Examination Survey [30]. Association with UFP exposure was tested using the Student's *T* test with $p < 0.05$ and Cohen's *d*.

MWAS of UFP exposure

Following reference standardization, we applied a multivariate MWAS framework to identify *m/z* features associated with UFP exposure. Partial least squares discriminant analysis (PLS-DA) was used for selection of exposure-associated features based upon low and high-exposure classification [31]. PLS components 1 through 3 were evaluated; the first two components were identified as the optimal number of latent components using the *plsgenomics* package [32]. Percent variability described by the first two components and R^2/Q^2 values support these components as optimal for the final model. The addition of the third component resulted in $R^2 \gg Q^2$, which suggests overfitting. *MixOmics* was used to build the final PLS-DA model and select discriminatory features based on variable importance for projection (VIP) score ≥ 2.0 [33]. Model accuracy was evaluated by R^2/Q^2 for PLS components 1 and 2, 10-fold cross-validation accuracy and random data predictive accuracy, which was calculated using the R package, xMSpanda (https://github.com/kuppal2/xmsPANDA).

Metabolite annotation

The *m/z* features were annotated using a three step process with final identification level based upon Schymanski, Jeon et al. [34]. First, detected *m/z* and retention time were compared to a database of approximately 150 metabolites with adduct mass and retention time confirmed by authentic reference standards (Level 1). Level 2 matches were not considered since MS/MS data were not collected for the majority of detected signals. Features not identified by comparison to the reference list were then annotated using HMDB in conjunction with xMSannotator [35], which uses a scoring system based upon correlation modularity clustering combined with isotopic, adduct and mass defect grouping to improve annotation of high-resolution mass spectrometry data (Level 3). The remaining *m/z* features were then matched using *m/z* alone and common adducts (Level 4) for positive and negative ESI using HMDB and METLIN [36]; *m/z* values providing no matches in either of the databases were considered non-identifiable chemical signals (Level 5). Non-identifiable signals are often present in untargeted HRM studies and can include uncharacterized environmental exposures or unknown metabolic intermediates [37]. All metabolite matching was completed using 10 parts-per-million (ppm) accuracy.

Metabolome correlation and pathway enrichment

To identify systemic effects associated with UFP exposure, we combined a network-based metabolome-wide correlation analysis of PLS-DA discriminatory metabolites with metabolic pathway enrichment. Pearson correlation and corresponding *p* between *m/z* features in the raw data and PLS-DA selected features were calculated pairwise using the R package MetabNet [38]. The *m/z* features with Pearson $|r| \geq 0.6$ and Benjamini-Hochberg FDR ≤ 5% [39] were selected for visualization in Cytoscape [40] and metabolic pathway enrichment using Mummichog [41].

Results

Study population

Demographics of the 59 CAFEH participants selected for HRM profiling are provided in Table 1. Age, sex, BMI, treatment for diabetes and statin use were comparable for the two exposures while education level differed ($p = 0.007$). As expected, UFP levels were significantly different ($p < 0.0001$). Since assignment to the low-exposure and high-exposure group was based upon personal time-adjusted and activity-adjusted UFP exposure, individuals from both neighborhoods were present in the two exposure groups. However, there was a significant difference ($p < 0.0001$) between residence location, with the majority of low-exposed individuals resided in Dorchester and South Boston, while high-exposed individuals lived in Somerville. Residence Euclidean distance to the nearest highway also differed between the two groups ($p = 0.02$), although the majority of individuals from both exposure categories lived within 100–500 m of the nearest highway.

High-resolution metabolomics

HRM profiling detected 8554 unique *m/z* features with mean replicate CV of 23% using HILIC chromatography with positive ESI and 6337 unique *m/z* features with mean replicate CV of 19% using RPC with negative ESI mode. Previous comparison of these analytical modes has shown the use of two ionization methods provides complementary detection of metabolites with limited overlap since different functional groups preferentially form adducts in either positive or negative ionization mode [22]. To confirm the measures from the two analytical modes were independent, we calculated the pairwise Pearson correlation coefficient between all HILIC and RPC *m/z* features used in the untargeted analysis (Supplementary Figure 1). Pearson correlation coefficient for 95% of the *m/z* features ranged between −0.27 and 0.37; less than 1% exhibited $|r| \geq 0.9$. Thus, due to different adducts, retention characteristics, ionization efficiency and limited correlation between intensities for the two modes, each dataset was tested for association with UFP independently. Prior to untargeted comparison of low and high exposure, *m/z* features detected

Table 1 Population characteristics and UFP exposure levels

Characteristic	Total	Low exposure	High exposure	*p*
Number of individuals	59	28	31	
Mean PNC ± SD	20,000 ± 4400	16,000 ± 2000	24,000 ± 2600	<0.0001
Sex				
Female	30	13	17	0.70
Male	29	15	14	
Age				
≤50	25	15	10	0.16
>50	34	13	21	
Statin use	14	4	10	0.28
Diabetes Medication Use	3	0	3	0.32
Neighborhood				
Somerville	28	6	22	<0.0001
Dorchester & South Boston	31	26	5	
BMI				
Normal (<25)	22	12	10	0.51
Overweight (25–30)	19	7	12	
Obese (>30)	18	9	9	
Education				
Less than high school diploma	10	1	9	0.007
Highschool diploma	12	5	7	
Undergraduate degree	22	10	12	
Graduate degree	15	12	3	
Orthogonal distance to highway (m)				
<50	9	1	8	0.02
50–100	7	4	3	
100–500	32	14	18	
>500	11	9	2	

in less than 80% of individuals in both groups were removed, resulting in 5367 and 3781 remaining for HILIC and RPC, respectively.

Reference standardization

To evaluate the metabolic effects of year-long UFP exposure, we first used a reference standardization approach to measure levels of central metabolic intermediates and test for differences between the low-exposure and high-exposure groups. Quantitative data on the association of metabolites critical to metabolic homeostasis and clinical health markers provide an important reference for how UFP exposure influence metabolic health. Thus, we provide measured concentrations for all 79 metabolites and concentration ranges reported in the Human Metabolome Database [7] in Tables 2 and 3, regardless of whether they reached the significance threshold. The results for amino acids, related metabolites and clinical health markers are provided in Table 2. The amino acids arginine, aspartic acid, cystine and glutamine, and the amino acid metabolite methionine sulfoxide differed at $p < 0.05$. None of the clinical health markers showed statistically significant differences at $p < 0.05$; however, the effect size measure (Cohen's $|d| > 0.3$) suggests possible variations in creatinine and histamine levels for the high-exposure group.

Reference standardization results for metabolites related to fatty acid metabolism, lipids, the tricarboxylic acid (TCA) cycle, nucleotides and co-factor metabolism are provided in Table 3. None of the measured metabolites were different between the low-exposure and high-exposure groups at $p < 0.05$. While not meeting the significance threshold of $p < 0.05$, the observed differences suggest positive associations with linolenic acid and niacin in the high-exposure group, while carnitine, acetyl-carnitine, myristic acid, palmitic acid, DHA, hypoxanthine, succinic acid, malic acid and citric acid were elevated in the low-exposure group.

Metabolome-wide association study of UFP exposure

To identify additional metabolic changes associated with UFP exposure, we applied PLS-DA to select discriminatory *m/z* features within the complete HRM dataset. Results from HILIC with positive ESI identified 178 *m/z* features. The resulting model exhibited good classification accuracy (Fig. 1a), with R^2/Q^2 values of 0.67/0.67 and 0.77/0.34 for PLS components 1 and 2, respectively. Support vector machine (SVM), 10-fold cross-validation balanced accuracy rate was 98.75% with mean permuted accuracy of 45.6%. Metabolite annotation identified 103 *m/z* features matching 136 unique chemicals. This included seven confirmed metabolites (Level 1); 42 metabolites identified based upon adduct and isotopic pairing (Level 3), and 85 based upon matching alone (Level 4). The remaining 70 detected *m/z* features provided no matches (Level 5). Due tothe large number of identified metabolites meeting the PLS-DA threshold, the identified metabolites consistent with risk factors for cardiopulmonary disease and environmental chemical exposure biomarkers for polycyclic aromatic hydrocarbons (PAH) and nicotine exposure are provided in Table 4; the full results are listed in Supplementary Table 1. Since education level differed between the low- and high-exposed groups, we performed a second untargeted MWAS using education level as the outcome

Table 2 Measured concentrations for amino acid, amino acid metabolites and clinical health marker levels

Metabolite[a]	All participants mean ± SD	Low exposure mean ± SD	High exposure mean ± SD	HMDB range	Cohen's *d*	*p*
Amino acids						
Alanine	206 ± 145	178 ± 116	231 ± 164	259–607	0.37	0.16
Arginine*	35 ± 14	31 ± 13	38 ± 14	60–224	0.57	0.032
Asparagine	33 ± 16	33 ± 15	32 ± 17	16–57	−0.08	0.76
Aspartic acid*	10 ± 7	12 ± 7	8 ± 5	16–26	−0.65	0.014
Citrulline	27 ± 14	26 ± 13	29 ± 14	27–38	0.17	0.51
Cystine*	103 ± 46	88 ± 35	117 ± 51	36–90	0.68	0.012
Glutamic acid	43 ± 18	44 ± 18	41 ± 19	24–151	−0.17	0.52
Glutamine*	765 ± 293	679 ± 334	844 ± 228	396–645	0.58	0.029
Histidine	52 ± 20	53 ± 20	52 ± 20	75–143	−0.08	0.76
Leucine/Isoleucine	260 ± 202	265 ± 226	255 ± 182	155–355	−0.05	0.86
Lysine	162 ± 59	156 ± 70	167 ± 49	178–456	0.18	0.50
Methionine	23 ± 10	21 ± 5	25 ± 13	22–46	0.36	0.18
Ornithine	13 ± 6	14 ± 7	13 ± 5	53–135	−0.13	0.61
Phenylalanine	60 ± 16	58 ± 18	62 ± 14	48–169	0.21	0.41
Proline	213 ± 188	200 ± 172	225 ± 203	168–239	0.13	0.62
Serine	55 ± 17	54 ± 14	57 ± 20	42–238	0.19	0.47
Taurine	141 ± 42	144 ± 51	139 ± 33	42–198	−0.13	0.62
Threonine	122 ± 36	119 ± 34	124 ± 38	102–260	0.15	0.58
Tryptophan	58 ± 18	58 ± 17	58 ± 19	37–60	0	1.00
Tyrosine	59 ± 16	58 ± 17	60 ± 15	54–144	0.13	0.62
Valine	194 ± 117	185 ± 89	202 ± 139	178–260	0.15	0.58
Amino acid metabolites						
5-Hydroxy-l-trytophan (nM)	17 ± 5	17 ± 6	16 ± 5	16–20	−0.09	0.73
Hippurate	1.2 ± 1.8	1.5 ± 2	0.9 ± 1.3	0–5	−0.30	0.25
Homocysteine	3 ± 5	3 ± 3	4 ± 6	6–12	0.18	0.50
Kynurenine	2.7 ± 1	2.8 ± 1.2	2.6 ± 0.8	0.7–3	−0.11	0.68
Methionine sulfoxide**	1.8 ± 0.5	1.6 ± 0.4	1.9 ± 0.5	3–5	0.72	0.008
Methyl-histidine	4 ± 3	4 ± 3	3 ± 3	0–12	−0.22	0.40
Acetyl-D-Tryptophan (nM)	148 ± 161	155 ± 164	142 ± 161	NA	−0.08	0.76
Oxoproline	40 ± 21	42 ± 22	39 ± 21	13–161	−0.18	0.49
Phenylpyruvic acid	1.2 ± 0.3	1.2 ± 0.3	1.3 ± 0.3	0.5–0.6	0.38	0.15
Clinical markers						
Lactic acid	903 ± 745	797 ± 589	999 ± 861	740–2400	0.27	0.30
Glucose (mM)	4.3 ± 1.3	4.304 ± 1.4	4.2 ± 1.3	3.9–6.1	−0.05	0.86
Cortisol (nM)	414 ± 265	418 ± 302	410 ± 232	28–660	−0.03	0.92
Cholesterol (mM)	3.9 ± 2.5	3.7 ± 2.5	4.1 ± 2.5	4.5–7	0.14	0.58
Creatinine	88 ± 38	94 ± 40	83 ± 37	56–109	−0.29	0.27
Urea (mM)	3.6 ± 2.3	3.9 ± 2.6	3.3 ± 1.91	4–9	−0.27	0.30
Creatine	19 ± 14	17 ± 8	21 ± 17	8.4–65	0.36	0.18
Uric acid	241 ± 85	248 ± 79	234 ± 90	238–506	−0.16	0.55
Histamine (nM)	22 ± 9	20 ± 9	24 ± 9	0.31–2.2	0.41	0.12

*$p < 0.05$; **$p < 0.01$

[a]Concentrations are given in μM unless noted otherwise

Table 3 Measured concentrations for fatty acid and lipid metabolism, nucleotides, the tricarboxylic acid cycle metabolites and co-factors

Metabolite[1]	All participants mean ± SD	TAA UFP < 19,000 mean ± SD	TAA UFP > 19,000 mean ± SD	Reference range	Cohen's *d*	*p*
Fatty acid and lipid metabolism						
Carnitine	38 ± 22	42 ± 23	35 ± 21	26–79	−0.33	0.21
Lauric acid	25 ± 17	23 ± 13	27 ± 20	2–36	0.24	0.36
Acetyl-carnitine	2 ± 1	3 ± 2	2 ± 0.9	3–8	−0.38	0.14
Myristoleic acid	18 ± 16	17 ± 16	18 ± 15	2–19	0.06	0.82
Myristic acid	65 ± 73	83 ± 91	49 ± 49	58–248	−0.47	0.07
Palmitoleic acid	256 ± 224	243 ± 185	267 ± 257	105–454	0.11	0.68
Palmitic acid (mM)	1.8 ± 1.1	2.0 ± 1.3	1.6 ± 0.8	1.9–3	−0.36	0.17
Margaric acid	1.2 ± 1.1	1.2 ± 1.05	1.2 ± 1.1	1–3	0.01	0.98
Gamma/alpha-Linolenic acid	54 ± 38	45 ± 26	63 ± 45	24–86	0.48	0.08
Linoleic acid (mM)	2.9 ± 1.6	2.7 ± 1.4	3.1 ± 1.7	2.6–4.6	0.28	0.28
Oleic acid (mM)	1.8 ± 1.2	1.6 ± 1.0	1.8 ± 1.3	1.4–3.2	0.19	0.46
Stearic acid	591 ± 431	628 ± 384	559 ± 474	515–939	−0.16	0.54
Eicosapentaenoic acid (nM)	447 ± 345	438 ± 369	454 ± 328	400–1800	0.05	0.86
Arachidonic acid	1001 ± 639	1080 ± 817	929 ± 422	538–1070	−0.23	0.37
Homo-gamma-Linolenic acid	140 ± 75	132 ± 71	146 ± 79	98–232	0.18	0.49
11,14-Eicosadienoic acid (nM)	305 ± 246	294 ± 258	315 ± 239	250–580	0.09	0.74
Eicosenoic acid	22 ± 58	23 ± 49	21 ± 66	9–22	−0.03	0.91
Docosahexaenoic acid	333 ± 312	383 ± 419	288 ± 162	72–227	−0.30	0.25
Docosapentaenoic acid	53 ± 28	52 ± 29	54 ± 28	26–59	0.08	0.77
Adrenic acid (nM)	440 ± 321	453 ± 353	429 ± 294	50–1500	−0.07	0.77
Respolvin E2 (nM)	0.15 ± 0.16	0.14 ± 0.19	0.15 ± 0.14	2–11	0.04	0.89
Leukotriene B4 (pM)	5 ± 10	4.7 ± 12	5.1 ± 8	0–600	0.04	0.89
Glycerophosphocholine	1.1 ± 1	1.2 ± 1	1.1 ± 0.9	NA	−0.09	0.72
Sphingosine	0.95 ± 0.8	1 ± 0.8	0.9 ± 0.8	0.049–0.51	−0.12	0.64
Sphinganine (nM)	2 ± 4	2 ± 5	2 ± 4	10–11	−0.10	0.69
Nucleotide metabolism						
5,6-Dihydrouracil (nM)	742 ± 362	775 ± 394	712 ± 334	20–1600	−0.17	0.51
Hypoxanthine	3 ± 4	4 ± 5	2 ± 2	1.3–54.5	−0.37	0.15
Xanthine (nM)	560 ± 1135	720 ± 1641	416 ± 154	200–800	−0.26	0.31
Uridine	5 ± 3	5 ± 3	4 ± 2	2.9–3.3	−0.23	0.38
TCA cycle metabolites						
Pyruvic acid	33 ± 14	34 ± 16	32 ± 12	22–258	−0.19	0.47
Succinic acid	8 ± 1	8 ± 1	8 ± 1	0–32	−0.34	0.20
Malic acid	1.4 ± 0.7	1.5 ± 0.6	1.3 ± 0.7	NA	−0.31	0.23
Citric acid	98 ± 52	109 ± 58	89 ± 44	55–121	−0.39	0.13
Vitamins and co-factors						
Pyridoxal (nM)	0.12 ± 0.12	0.1 ± 0.1	0.13 ± 0.15	0.2–0.3	0.21	0.43
Pantothenic acid	19 ± 29	20 ± 24	18 ± 33	4.5–5.3	−0.06	0.83
Alpha-tocopherol	16 ± 9	16 ± 9	15 ± 9	18–44	−0.02	0.94
Tetrahydrofolic acid (nM)	9 ± 4	9 ± 4	8 ± 3	0–7	−0.11	0.67
Choline	1.3 ± 0.5	1.3 ± 0.5	1.3 ± 0.6	6.5–12.5	−0.01	0.97
Niacin	6 ± 14	4 ± 11	8 ± 16	43–55	0.34	0.20
Methylnicotinic acid (nM)	15 ± 34	19 ± 49	11 ± 8	NA	−0.24	0.35

[a]Concentrations are given in μM unless noted otherwise

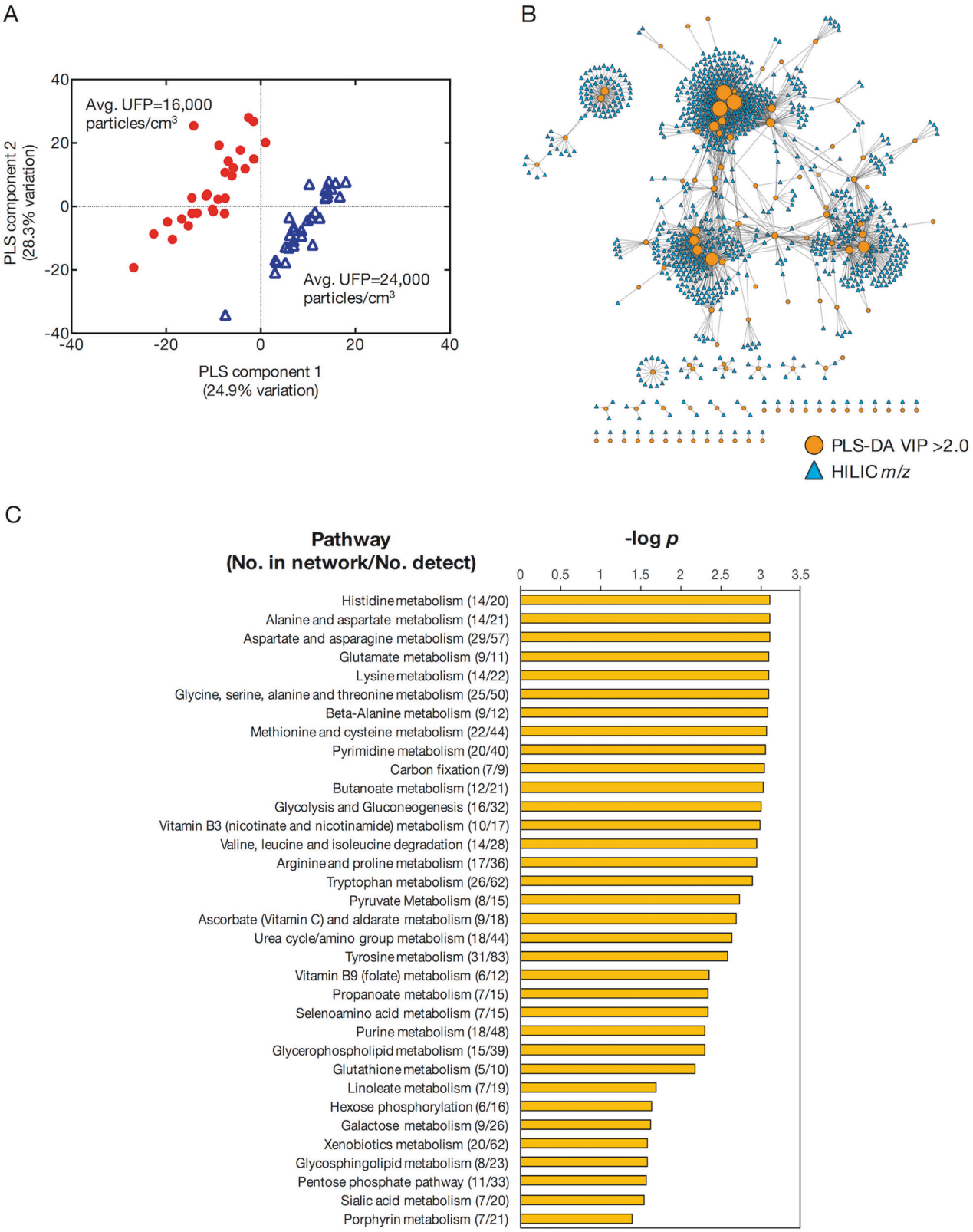

variable. Using the same VIP threshold, 64 *m/z* features were identified and did not include any of the 178 *m/z* features discriminating low-UFP exposure from high-UFP exposure.

◀ **Fig. 1** Metabolome-wide association study of UFP exposure using HILIC HRM data. **a** PLS-DA identified 178 *m/z* features discriminating CAFEH participants with low and high exposure, clearly separating the two groups. **b** Metabolic network structure using PLS-DA selected features and raw HILIC data identified an additional 928 *m/z* features strongly correlated with the discriminatory metabolites. Correlation network data was then used to evaluate metabolic pathway enrichment. **c** Metabolic pathways associated with exposure correlation network using HILIC with positive ESI at $p < 0.05$

Comparison of *m/z* features from RPC with negative ESI also showed metabolic associations with UFP exposure. PLS-DA identified 138 *m/z* features discriminating between low-exposure and high-exposure. The selected features provided good classification accuracy (Fig. 2a), with R^2/Q^2 of 0.73/0.72 and 0.83/0.38 for PLS components 1 and 2, respectively. The 10-fold cross-validation balanced accuracy rate was 98.75% with mean permuted accuracy of 55.2%. Annotation resulted in 74 *m/z* features matching 83 unique metabolites. This included four confirmed metabolites, five metabolites meeting Level 3 identification criteria, and 74 matches based upon Level 4. The remaining 64 *m/z* features provided no matches (Level 5). Metabolites identified by RPC with negative ESI included amino acids, endothelial function related metabolites, co-factors and environmental chemicals arising from exposure to PAHs and nicotine; only identified metabolites related to cardiopulmonary disease risk factors and environmental chemical exposure biomarkers are provided in Table 5; the complete annotation results for RPC with negative ionization are listed in Supplementary Table 2. A second MWAS using education level as the outcome variable identified 152 *m/z* at VIP ≥ 2.0, six of which were also identified in the UFP analysis. These *m/z* features included a match to bromomethane, PS(16:018:0), dihydroorotic acid, hydroxyfluoroprednisolone butyrate, fucose and one unidentifiable *m/z* signal ($m/z = 217.8614$).

Metabolite correlation and pathway enrichment

Following identification of PLS-DA selected *m/z* features, a metabolome-wide Pearson correlation analysis was completed by testing for additional associations within the raw data. Combined with pathway enrichment in Mummichog, this approach improves detection of metabolic changes associated with exposure while reducing false positives due to the use of a random sampling permutation approach for annotation and pathway mapping. The correlation networks for HILIC with positive ESI and RPC with negative ESI are provided in Figs. 1b and 2b, respectively. For HILIC, an additional 928 *m/z* features were correlated with the PLS-DA results. Pathway enrichment showed exposure-associated alterations in 34 different metabolic pathways that had five or more annotated metabolites within the correlation network (Fig. 1c). These included pathways related to amino acids, oxidative stress, nucleotide metabolism, cofactors, xenobiotics, and fatty acid metabolism.

A similar correlation network was obtained for RPC, which included an additional 721 *m/z* features. Pathway enrichment results are shown in Fig. 2c. Sixteen pathways were identified as associated with UFP exposure, including amino acid pathways, microbiome-related metabolites, fatty acid metabolism, cofactors, nucleotide metabolism, and the TCA cycle.

Discussion

Although long-term exposure to air pollution has been associated with cardiopulmonary diseases, the underlying mechanisms and mode of action are unknown. In this study, we applied HRM to identify metabolic changes associated with year-long averaged personal UFP exposure. Initial characterization of amino acids, clinical markers, lipid/fatty acid metabolites, co-factors and cellular respiration was completed to assess exposure-associated changes to key metabolic intermediates. This analysis was followed by identification of global metabolomic differences between the two groups at the metabolite and pathway level.

By providing absolute concentrations of metabolites, the use of reference standardization allows evaluation of physiological levels of central human metabolites and comparison to expected ranges [26]. In this study, concentrations of 79 metabolites were determined. Compared to HMDB, 26 were outside reported ranges, including 17 that were lower than previously reported concentrations. While this population was differentiated into low-exposure and high-exposure groups, as a whole the CAFEH cohort may carry a higher burden of UFP exposure due to residential proximity to highways within an urban area. Thus, exposure history could contribute to the differences between metabolite concentrations measured in CAFEH participants and those listed in HMDB.

Comparison of the metabolite levels between the low and high-exposure groups identified five metabolites significantly different at $p < 0.05$. Elevated methionine sulfoxide (MetSO) and cystine (CySS) are consistent with increased oxidative stress. In humans, the major extracellular thiol/disulfide redox couple is cysteine and its disulfide form, CySS [42]. Increased oxidation of this couple and subsequent shift towards a more positive redox potential has been shown to result in activation of pro-inflammatory cytokines [43], regulate early events in atherosclerosis [44] and is associated with cardiovascular disease and endothelial function [45]. MetSO is the oxidation product of methionine with reactive oxygen species and

Table 4 Select annotated metabolites detected using HILIC with positive ESI identified by cross-sectional PLS-DA low- and high-UFP exposure

m/z	Adduct	Identity	Identification confidence[a]	VIP	Cohen's *d*	*p*
134.0450	M + H	L-Aspartic acid	1	2.56	−0.73	0.007
279.2322	M + H	Alpha/gamma-Linolenic acid	1	2.22	−0.62	0.021
166.0534	M + H	Methionine sulfoxide	1	2.46	0.70	0.010
241.0314	M + H	L-Cystine	1	2.61	0.74	0.006
134.0190	M + 2Na-H	Alanine	1	2.59	0.74	0.006
129.1024	M + H-H2O	L-Lysine	1	2.71	0.78	0.004
169.0586	M + Na	L-Glutamine	1	3.35	1.01	2.98E-04
157.1225	M + H	4-Hydroxynonenal	3	2.17	0.60	0.024
225.1324	M + Na	Dimethylarginine	3	2.79	0.79	0.003
217.0821	M + ACN + Na	FAPy-adenine	4	2.58	−0.74	0.006
233.0788	M + ACN + H	gamma-Carboxyglutamic acid	4	2.40	−0.68	0.012
261.1448	M + ACN + H	Pantothenic acid	4	2.01	0.54	0.037
376.0578	M + K	S-(Hydroxymethyl) glutathione	4	2.12	0.59	0.027
335.1255	M + H-H2O	Cotinine glucuronide	4	2.25	0.64	0.019
347.0650	M + 2Na-H	Benzo(a)pyrene diol epoxide	4	2.33	0.65	0.015
337.1047	M + Na	7,8-Dihydropteroic acid	4	2.55	0.72	0.007
279.1116	M + ACN + Na	Acetyl vitamin K5	4	3.17	0.94	6.76E-04

VIP variable importance projection score

[a]Identification confidence based upon Schymanski et al. (2014)

a recognized marker of oxidative stress [46, 47]. Changes in arginine (Arg), aspartate (Asp) and glutamine (Gln) suggest alterations to critical processes for endothelial function. Gln is a precursor for de novo synthesis of Arg through intestinal uptake of Gln and release of citrulline, which is then converted to Arg at the kidney [48]. Arg is a direct precursor of nitric oxide (NO), which is generated in the endothelium by endothelial NO synthase [49]. Changes in NO production result in disruption to vascular homeostasis, and have been implicated in a wide range of pathological states [50]. These findings are consistent with other metabolic profiling studies of air pollution, which showed associations of exposure to $PM_{2.5}$ and ozone with decreased Arg and elevated Asp [9, 10].

Cross-sectional comparison using all detected *m/z* features identified complementary metabolic changes associated with UFP. In addition to Gln, Asp, MetSO and CySS, PLS-DA identified other metabolic intermediates quantified by reference standardization, including linolenic acid, alanine (Ala), lysine (Lys), glutamate (Glu) and threonine (Thr). The observed changes for linolenic acid and Thr were consistent with associations observed in MWAS of benzo [a]pyrene [51]; decreases in linolenic acid and Glu provide additional evidence of oxidative stress related changes. Glu is a precursor for glutathione, the second major thiol redox couple for antioxidant defense. Linoleic acid is an isomeric polyunsaturated fatty acid that includes an omega-3 (alpha-linolenic acid) and omega-6 (gamma-linolenic acid) species. Polyunsaturated fatty acids are susceptible to lipid peroxidation, which occurs through oxidant attack at carbon-carbon bonds with subsequent hydrogen abstraction and oxygen insertion [52]. Increased oxidative stress and formation of in vivo ROS has been well documented in exposure to particulate matter [53, 54]. Elevated 4-hydroxynonenal (4-HNE), a lipid peroxidation biomarker, supports increased formation of ROS. 4-HNE is a relatively stable, major aldehyde product formed during lipid peroxidation that exhibits cytotoxicity and reacts with a wide range of different biomolecules, including proteins, lipids and nucleic acids [55]. Lipid peroxidation products have also been implicated as a pro-inflammatory signaling molecule and in the pathogenesis of multiple diseases [56, 57].

Metabolites consistent with increased risk for endothelial dysfunction were also identified. Both dimethylarginine and agmatine have the potential to inhibit NO synthase and were increased with UFP exposure. Dimethylarginine (DMA) exists in an asymmetric (ADMA) and symmetric (SDMA) form; due to the chromatography technique used in this study it was not possible to separate the two isomers and the measured intensity represents the sum of the two. Both ADMA and SDMA form through enzymatic methylation of arginine residues, which is catalyzed by S-adenosylmethionine protein N-methytransferase and

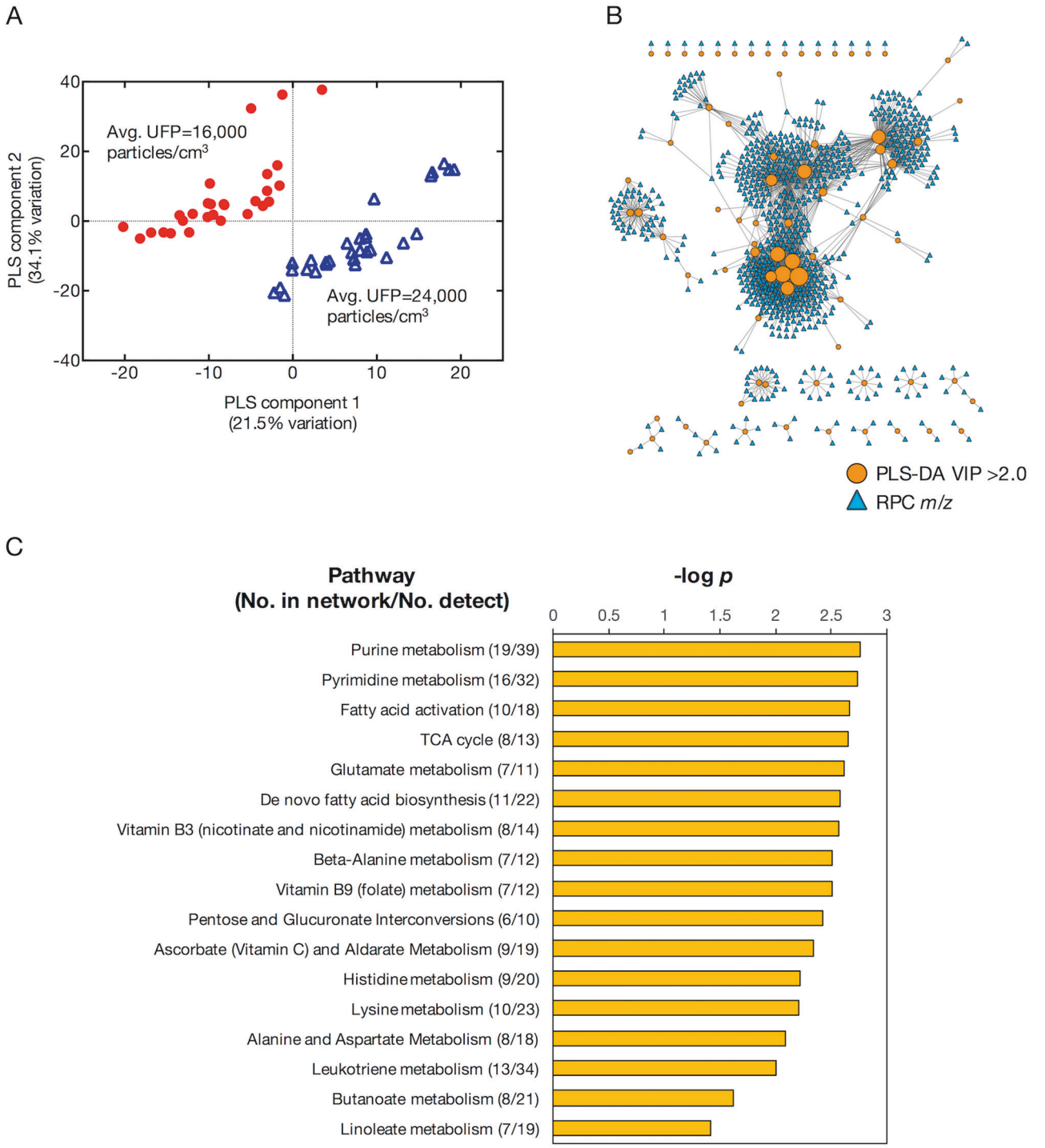

Fig. 2 Metabolome-wide association study of UFP exposure using C_{18} with negative ESI HRM data. **a** PLS-DA identified 138 *m/z* features discriminating CAFEH participants with low and high exposure, providing clear separation between the two groups. **b** The metabolic correlation network identified an additional 721 *m/z* features meeting the correlation and *p* thresholds, which was then evaluated for metabolic pathway enrichment. **c** Metabolic pathways associated with exposure correlation network using RPC with negative ESI at $p < 0.05$

methylated by S-adenosylmethionine (SAMe). ADMA is a competitive inhibitor of NO synthase that can result in arginine deficiency and disruption to endothelial homeostasis [58]. ADMA has been linked to risk factors for cardiovascular disease, including hyperhomocysteinemia, hypercholesterolemia, obesity and inflammation [59, 60]. While not directly inhibiting NO, SDMA competes with arginine for endothelial transporters, and has been shown to

Table 5 Select annotated metabolites detected using RPC with negative ESI identified by cross-sectional PLS-DA low- and high-UFP exposure

m/z	Adduct	Identity	Identification confidence[a]	VIP	Cohen's *d*	*p*
197.0684	M + Na-2H	Cotinine	1	2.43	−0.69	0.013
132.0305	M-H	L-Aspartic acid	1	2.48	−0.68	0.011
128.0355	M-H2O-H	L-Glutamic acid	1	2.03	−0.55	0.039
118.0512	M-H	L-Threonine	1	2.06	0.55	0.036
151.0404	M-H	3,4-Dihydroxyphenylacetaldehyde	3	2.14	−0.57	0.029
272.4254	M-3H	3-Sialyl Lewis	4	2.17	−0.59	0.027
107.0504	M-H	Cresol	4	2.01	0.53	0.041
289.1216	M-H	trans-dimethylbenz(a)anthracene -5,6-dihydrodiol	4	2.01	0.54	0.041
494.1544	M + Cl	5-Methyltetrahydrofolic acid	4	2.05	0.55	0.037
165.0924	M + Cl	Agmatine	4	2.43	0.68	0.013
157.0509	M + Na-2H	Tetrahydropteridine	4	2.67	0.73	0.006
445.2942	M-H	24-Oxo-1alpha2325-trihydroxyvitamin D3	4	2.82	0.78	0.003
475.1970	M-H	2-Methoxyestrone 3-glucuronide	4	2.80	0.78	0.004
322.9821	M + Na-2H	Ellagic acid	4	2.83	0.79	3.38E-03

VIP variable importance projection score

[a]Identification confidence based upon Schymanski et al. (2014)

reduce NO production in intact endothelial cells [61]. Agmatine, which is a decarboxylation product of arginine, inhibits inducible NO synthase and acts as a modulator of NO production [62]. 5-methyltetrahydrofolic acid (5-MTHF) is the most biologically active form of folic acid and was associated with UFP. 5-MTHF has been implicated in dysregulation of homocysteine levels and identified as a tentative biomarker of cardiovascular disease [63].

In addition to changes in endogenous metabolites, chemical biomarkers of exposure to air pollution were positively correlated with UFP exposure. These included two PAH metabolites, benzo(a)pyrene diol epoxide (BPDE) and trans-dimethylbenz(a)anthracene-5,6-dihydrodiol (tDMBA-DH). BPDE is a chemical carcinogen formed through oxidation of benzo[a]pyrene, resulting in a metabolically active species [64, 65]. tDMBA-DH is a precursor to the metabolically active, dipole epoxide metabolite of dimethylbenz(a)anthracene (DMBA). Similar to benzo[a]pyrene, DMBA is a recognized carcinogen, with modes of action including formation of DNA adducts through binding to dAdo and dGuo DNA residues [66]. Cresols, which include three different isomers (para-, meta-, ortho-), are combustion products widely distributed throughout the environment. Sources include automobile exhaust, tobacco smoke and combustion of organic materials, with concentrations largely dependent on the distance from the source due to degradation in the atmosphere [67]. Although participant selection was biased towards non-smokers, the nicotine metabolites cotinine and cotinine-glucuronide were detected. To assess if any individuals were active smokers, cotinine levels were quantified using reference standardization. Excluding two individuals from the low UFP exposure group with cotinine levels of 4.9 and 1.8 ng/mL, for all other participants cotinine was either not detected or below 1 ng/mL. A plasma cotinine level greater than 10 ng/mL is typically used to identify active smokers. Thus, cotinine levels suggest only passive exposure to cigarette smoke and were at low levels in all but two samples.

Disease typically manifests as disruption to homeostatic control, and understanding systemic changes associated with exposure can improve insight into the mechanisms underlying exposure-related diseases. Pathway enrichment analyses showed systemic changes to a range of biochemical processes, including oxidative stress and endothelial function. Pathways altered with exposure included sulfur amino acid metabolism, linoleate metabolism, glutamate and arginine/proline metabolism. In addition, seven metabolites from porphyrin metabolism were identified using HILIC. Porphyrins are critical co-factors for the synthesis of hemoglobin; alterations in hemoglobin to levels outside normal physiological range has been associated with increased risk for cardiac events [68]. Additional metabolic alterations associated with UFP exposure important to human health include inflammatory processes (leukotriene

metabolism), the microbiome (sialic acid metabolism, propionate metabolism and butanoate metabolism), mitochondrial bioenergetics (pentose phosphate pathway, fatty acid activation, TCA cycle, pyruvate metabolism, glycolysis and gluconeogenesis), co-factor metabolism (vitamin B3, vitamin B9 and ascorbate/aldarate metabolism) and nucleotide metabolism (purine and pyrimidine metabolism). Thus, these results show exposure-associated metabolic variations were present for the biochemical processes that are central in maintaining homeostasis and health; additional characterization will be needed to evaluate if these alterations occur to an extent consistent with disease and to show causal relationships.

We acknowledge several limitations of this study. As a whole, this population presumably carries a higher burden of exposure to traffic-related air pollution than residents in suburban and rural areas. Second, participant selection excluded smokers and was designed for cross-sectional comparison of low and high UFP exposures. The results from this study represent a population averaged response to UFP exposure. We could not evaluate how short-term, daily exposures influence intra-individual variation in response to air pollution, or evaluate the effect of circadian rhythm. Metabolism has long been known to exhibit diurnal cycles that could influence response to traffic-related air pollution, with time of day, amount of sleep, timing of meals, and light–dark cycles associated with metabolic fluctuations for control of energy expenditure and intake distribution during the waking period [69]. In addition, the results from this study are correlative in nature. We could not account for unknown confounders, other unanticipated exposures associated with traffic, living in these neighborhoods or indoor generation of UFP from other sources, such as cooking or heating, nor identify the exact mechanism through which these metabolic associations occurred. Third, while confidence-based methods were used for annotation of metabolites, unidentifiable signals were not extensively characterized. Despite these limitations, we identified UFP associated changes to the metabolic phenotype. The results demonstrate the use of HRM as a viable platform for untargeted characterization of molecular mechanisms underlying environmental exposures and represent one of the first metabolomic characterizations of long-term exposure to air pollution.

In the present study, we applied HRM to identify metabolic variations associated with near-highway exposures. Annual, personal UFP exposure was determined using high-resolution spatial-temporal models to predict PNC with time-activity adjustments, and metabolic differences were evaluated for participants with low and high exposure. We identified metabolic alterations associated with exposure that are consistent with inhibition of nitric oxide production and elevated oxidative stress. These alterations included a shift in the CyS/CySS couple towards a more positive steady-state redox potential, elevated dimethylarginine and elevated levels of 4-HNE, all of which are recognized risk factors for atherosclerosis, endothelial dysfunction and cardiovascular disease. Metabolic pathway enrichment suggests that long-term UFP exposure leads to systemic changes in a wide range of biochemical processes that have important implications for health. Taken together, the results from this study are consistent with long-term exposure to traffic-related air pollution leading to increased oxidative stress and changes to metabolic regulators of endothelial function.

Acknowledgements This work was supported by funds received from the National Institute of Health, award numbers ES019776, ES023485, ES025632, ES015462, and OD018006. The contents of this article do not necessarily reflect the views of HEI, or its sponsors, nor do they necessarily reflect the views and policies of the EPA or motor vehicle and engine manufacturers.

Compliance with ethical standards

Conflict of interest The authors declare that they have no conflict of interest.

References

1. Lim SS, Vos T, Flaxman AD, Danaei G, Shibuya K, Adair-Rohani H, et al. A comparative risk assessment of burden of disease and injury attributable to 67 risk factors and risk factor clusters in 21 regions, 1990-2010: a systematic analysis for the Global Burden of Disease Study 2010. Lancet. 2012;380:2224–60.
2. Di Q, Wang Y, Zanobetti A, Wang Y, Koutrakis P, Choirat C, et al. Air pollution and mortality in the medicare population. N Eng J Med. 2017;376:2513–22.
3. Zuurbier M, Hoek G, Oldenwening M, Meliefste K, van den Hazel P, Brunekreef B. Respiratory effects of commuters' exposure to air pollution in traffic. Epidemiology. 2011;22:219–27.
4. Fuller CH, Williams PL, Mittleman MA, Patton AP, Spengler JD, Brugge D. Response of biomarkers of inflammation and coagulation to short-term changes in central site, local, and predicted particle number concentrations. Ann Epidemiol. 2015;25:505–11.
5. Baccarelli A, Wright RO, Bollati V, Tarantini L, Litonjua AA, Suh HH, et al. Rapid DNA methylation changes after exposure to traffic particles. Am J Respir Crit Care Med. 2009;179:572–8.
6. Chu JH, Hart JE, Chhabra D, Garshick E, Raby BA, Laden F. Gene expression network analyses in response to air pollution exposures in the trucking industry. Environ Health. 2016;15:101.
7. Wishart DS, Jewison T, Guo AC, Wilson M, Knox C, Liu Y, et al. HMDB 3.0--The Human Metabolome Database in 2013. Nucleic Acids Res. 2013;41:D801–7.
8. Liu KH, Walker DI, Uppal K, Tran V, Rohrbeck P, Mallon TM, et al. High resolution metabolomics assessment of military personnel. J Occup Environ Med. 2016;58(8 Suppl 1):S53–61.
9. Breitner S, Schneider A, Devlin RB, Ward-Caviness CK, Diaz-Sanchez D, Neas LM, et al. Associations among plasma metabolite levels and short-term exposure to PM2.5 and ozone in a cardiac catheterization cohort. Environ Int. 2016;97:76–84.
10. Surowiec I, Karimpour M, Gouveia-Figueira S, Wu J, Unosson J, Bosson JA, et al. Multi-platform metabolomics assays for human

lung lavage fluids in an air pollution exposure study. Anal Bioanal Chem. 2016;408:4751–64.
11. Vlaanderen JJ, Janssen NA, Hoek G, Keski-Rahkonen P, Barupal DK, Cassee FR, et al. The impact of ambient air pollution on the human blood metabolome. Environ Res. 2017; 156:341–8.
12. Pradhan SN, Das A, Meena R, Nanda RK, Rajamani P. Biofluid metabotyping of occupationally exposed subjects to air pollution demonstrates high oxidative stress and deregulated amino acid metabolism. Sci Rep. 2016;6:35972.
13. Menni C, Metrustry SJ, Mohney RP, Beevers S, Barratt B, Spector TD, et al. Circulating levels of antioxidant vitamins correlate with better lung function and reduced exposure to ambient pollution. Am J Respir Crit Care Med. 2015;191:1203–7.
14. Lane KJ, Levy JI, Scammell MK, Peters JL, Patton AP, Reisner E, et al. Association of modeled long-term personal exposure to ultrafine particles with inflammatory and coagulation biomarkers. Environ Int. 2016;92-93:173–82.
15. Fuller CH, Patton AP, Lane K, Laws MB, Marden A, Carrasco E, et al. A community participatory study of cardiovascular health and exposure to near-highway air pollution: study design and methods. Rev Environ Health. 2013;28:21–35.
16. Patton AP, Zamore W, Naumova EN, Levy JI, Brugge D, Durant JL. Transferability and generalizability of regression models of ultrafine particles in urban neighborhoods in the Boston area. Environ Sci Technol. 2015;49:6051–60.
17. Lane KJ, Levy JI, Scammell MK, Patton AP, Durant JL, Mwamburi M, et al. Effect of time-activity adjustment on exposure assessment for traffic-related ultrafine particles. J Expo Sci Environ Epidemiol. 2015;25:506–16.
18. Patton AP, Perkins J, Zamore W, Levy JI, Brugge D, Durant JL. Spatial and temporal differences in traffic-related air pollution in three urban neighborhoods near an interstate highway. Atmos Environ. 1994;2014:309–21.
19. Lane KJ, Kangsen Scammell M, Levy JI, Fuller CH, Parambi R, Zamore W, et al. Positional error and time-activity patterns in near-highway proximity studies: an exposure misclassification analysis. Environ Health. 2013;12:75.
20. Fuller CH, Brugge D, Williams PL, Mittleman MA, Lane K, Durant JL, et al. Indoor and outdoor measurements of particle number concentration in near-highway homes. J Expo Sci Environ Epidemiol. 2013;23:506–12.
21. Soltow QA, Strobel FH, Mansfield KG, Wachtman L, Park Y, Jones DP. High-performance metabolic profiling with dual chromatography-Fourier-transform mass spectrometry (DC-FTMS) for study of the exposome. Metabolomics. 2013;9:S132–S143.
22. Liu KH, Walker DI, Uppal K, Tran V, Rohrbeck P, Mallon TM, et al. High-resolution metabolomics assessment of military personnel: evaluating analytical strategies for chemical detection. J Occup Environ Med / Am Coll Occup Environ Med. 2016;58: S53–61.
23. Yu T, Park Y, Li S, Jones DP. Hybrid feature detection and information accumulation using high-resolution LC-MS metabolomics data. J Proteome Res. 2013;12:1419–27.
24. Uppal K, Soltow QA, Strobel FH, Pittard WS, Gernert KM, Yu T, et al. xMSanalyzer: automated pipeline for improved feature detection and downstream analysis of large-scale, non-targeted metabolomics data. BMC Bioinforma. 2013;14:15.
25. Johnson WE, Li C, Rabinovic A. Adjusting batch effects in microarray expression data using empirical Bayes methods. Biostatistics. 2007;8:118–27.
26. Go YM, Walker DI, Liang Y, Uppal K, Soltow QA, Tran V, et al. Reference standardization for mass spectrometry and high-resolution metabolomics applications to exposome research. Toxicol Sci. 2015;148:531–43.
27. Simon-Manso Y, Lowenthal MS, Kilpatrick LE, Sampson ML, Telu KH, Rudnick PA, et al. Metabolite profiling of a NIST Standard Reference Material for human plasma (SRM 1950): GC-MS, LC-MS, NMR, and clinical laboratory analyses, libraries, and web-based resources. Anal Chem. 2013;85:11725–31.
28. Quehenberger O, Armando AM, Brown AH, Milne SB, Myers DS, Merrill AH, et al. Lipidomics reveals a remarkable diversity of lipids in human plasma. J Lipid Res. 2010;51:3299–305.
29. Colas RA, Shinohara M, Dalli J, Chiang N, Serhan CN. Identification and signature profiles for pro-resolving and inflammatory lipid mediators in human tissue. Am J Physiol Cell Physiol. 2014;307:C39–54.
30. CDC, NCHS. Laboratory Data: Brominated Flame Retardants (BFRs), Non-dioxin-like Polychlorinated Biphenyls, Fatty Acids - Plasma; Year 2003-2004. In: National Health and Nutrition Examination Survey Data, Year 2003-2004. August 2007, April 2008 ed. https://wwwn.cdc.gov/nchs/nhanes/Search/DataPage.aspx?Component=Laboratory&CycleBeginYear=2003; Accessed 21 Jan 2017: Centers for Disease Control and Prevention; National Center for Health Statistics.
31. Wold S, Sjöström M, Eriksson L. PLS-regression: a basic tool of chemometrics. Chemom Intell Lab Syst. 2001;58:109–30.
32. Boulesteix A, Durif G, Labmbert-Lacroix S, Peyre J, Strimmer K. plsgenomics: PLS Analyses for Genomics. In. R package version 1.3-2. https://CRAN.R-project.org/package=plsgenomics ed, 2017.
33. Rohart F, Gautier B, Singh A, Le Cao KA. mixOmics: an R package for 'omics feature selection and multiple data integration. PLoS Comput Biol. 2017;13:e1005752.
34. Schymanski EL, Jeon J, Gulde R, Fenner K, Ruff M, Singer HP, et al. Identifying small molecules via high resolution mass spectrometry: communicating confidence. Environ Sci Technol. 2014;48:2097–8.
35. Uppal K, Walker DI, Jones DP. xMSannotator: an R package for network-based annotation of high-resolution metabolomics data. Analytical chemistry 2016; https://doi.org/10.1021/acs.analchem.6b01214.
36. Smith CA, O'Maille G, Want EJ, Qin C, Trauger SA, Brandon TR, et al. METLIN: a metabolite mass spectral database. Ther Drug Monit. 2005;27:747–51.
37. Uppal K, Walker DI, Liu K, Li S, Go YM, Jones DP. Computational metabolomics: a framework for the million metabolome. Chemical research in toxicology 2016; https://doi.org/10.1021/acs.chemrestox.6b00179.
38. Uppal K, Soltow QA, Promislow DE, Wachtman LM, Quyyumi AA, Jones DP. MetabNet: an R package for metabolic association analysis of high-resolution metabolomics data. Front Bioeng Biotechnol. 2015;3:87.
39. Benjamini Y, Hochberg Y. Controlling the false discovery rate - a practical and powerful approach to multiple testing. J Roy Stat Soc B Met. 1995;57:289–300.
40. Su G, Morris JH, Demchak B, Bader GD. Biological network exploration with cytoscape 3. Curr Protoc Bioinforma. 2014;47:8 13 11-18 13 24.
41. Li S, Park Y, Duraisingham S, Strobel FH, Khan N, Soltow QA, et al. Predicting network activity from high throughput metabolomics. PLoS Comput Biol. 2013;9:e1003123.
42. Go YM, Jones DP. Cysteine/cystine redox signaling in cardiovascular disease. Free Radic Biol Med. 2011;50:495–509.
43. Iyer SS, Accardi CJ, Ziegler TR, Blanco RA, Ritzenthaler JD, Rojas M, et al. Cysteine redox potential determines pro-inflammatory IL-1beta levels. PLoS ONE. 2009;4:e5017.
44. Go YM, Jones DP. Intracellular proatherogenic events and cell adhesion modulated by extracellular thiol/disulfide redox state. Circulation. 2005;111:2973–80.

45. Ashfaq S, Abramson JL, Jones DP, Rhodes SD, Weintraub WS, Hooper WC, et al. Endothelial function and aminothiol biomarkers of oxidative stress in healthy adults. Hypertension. 2008;52:80–5.
46. Moskovitz J, Berlett BS, Poston JM, Stadtman ER. The yeast peptide-methionine sulfoxide reductase functions as an antioxidant in vivo. Proc Natl Acad Sci USA. 1997;94:9585–9.
47. Mashima R, Nakanishi-Ueda T, Yamamoto Y. Simultaneous determination of methionine sulfoxide and methionine in blood plasma using gas chromatography-mass spectrometry. Anal Biochem. 2003;313:28–33.
48. Ligthart-Melis GC, van de Poll MC, Boelens PG, Dejong CH, Deutz NE, van Leeuwen PA. Glutamine is an important precursor for de novo synthesis of arginine in humans. Am J Clin Nutr. 2008;87:1282–9.
49. Gornik HL, Creager MA. Arginine and endothelial and vascular health. J Nutr. 2004;134:2880S–2887S. discussion 2895S
50. Tousoulis D, Kampoli AM, Tentolouris C, Papageorgiou N, Stefanadis C. The role of nitric oxide on endothelial function. Curr Vasc Pharmacol. 2012;10:4–18.
51. Accardi CJ, Walker DI, Uppal K, Quyyumi AA, Rohrbeck P, Pennell KD, et al. High-resolution metabolomics for nutrition and health assessment of armed forces personnel. J Occup Environ Med. 2016;58:S80–8.
52. Yin H, Xu L, Porter NA. Free radical lipid peroxidation: mechanisms and analysis. Chem Rev. 2011;111:5944–72.
53. Lodovici M, Bigagli E. Oxidative stress and air pollution exposure. J Toxicol. 2011;2011:487074.
54. Bates JT, Weber RJ, Abrams J, Verma V, Fang T, Klein M, et al. Reactive oxygen species generation linked to sources of atmospheric particulate matter and cardiorespiratory effects. Environ Sci Technol. 2015;49:13605–12.
55. Weber D, Milkovic L, Bennett SJ, Griffiths HR, Zarkovic N, Grune T. Measurement of HNE-protein adducts in human plasma and serum by ELISA-Comparison of two primary antibodies. Redox Biol. 2013;1:226–33.
56. Akude E, Zherebitskaya E, Roy Chowdhury SK, Girling K, Fernyhough P. 4-Hydroxy-2-nonenal induces mitochondrial dysfunction and aberrant axonal outgrowth in adult sensory neurons that mimics features of diabetic neuropathy. Neurotox Res. 2010;17:28–38.
57. Selley ML. (E)-4-hydroxy-2-nonenal may be involved in the pathogenesis of Parkinson's disease. Free Radic Biol Med. 1998;25:169–74.
58. Sibal L, Agarwal SC, Home PD, Boger RH. The role of asymmetric dimethylarginine (ADMA) in endothelial dysfunction and cardiovascular disease. Curr Cardiol Rev. 2010;6:82–90.
59. Stuhlinger MC, Oka RK, Graf EE, Schmolzer I, Upson BM, Kapoor O, et al. Endothelial dysfunction induced by hyperhomocyst(e)inemia: role of asymmetric dimethylarginine. Circulation. 2003;108:933–8.
60. Eid HM, Arnesen H, Hjerkinn EM, Lyberg T, Seljeflot I. Relationship between obesity, smoking, and the endogenous nitric oxide synthase inhibitor, asymmetric dimethylarginine. Metabolism. 2004;53:1574–9.
61. Bode-Boger SM, Scalera F, Kielstein JT, Martens-Lobenhoffer J, Breithardt G, Fobker M, et al. Symmetrical dimethylarginine: a new combined parameter for renal function and extent of coronary artery disease. J Am Soc Nephrol. 2006;17:1128–34.
62. Raghavan SA, Dikshit M. Vascular regulation by the L-arginine metabolites, nitric oxide and agmatine. Pharmacol Res. 2004;49:397–414.
63. Jacobsen DW. Homocysteine and vitamins in cardiovascular disease. Clin Chem. 1998;44:1833–43.
64. Chung MK, Riby J, Li H, Iavarone AT, Williams ER, Zheng Y, et al. A sandwich enzyme-linked immunosorbent assay for adducts of polycyclic aromatic hydrocarbons with human serum albumin. Anal Biochem. 2010;400:123–9.
65. Delaney JC, Essigmann JM. Biological properties of single chemical-DNA adducts: a twenty year perspective. Chem Res Toxicol. 2008;21:232–52.
66. Sobinoff AP, Mahony M, Nixon B, Roman SD, McLaughlin EA. Understanding the Villain: DMBA-induced preantral ovotoxicity involves selective follicular destruction and primordial follicle activation through PI3K/Akt and mTOR signaling. Toxicol Sci. 2011;123:563–75.
67. ATSDR. Toxicological Profile for Cresols. Atlanta, GA: Agency for Toxic Substances and Disease Registry, Division of Toxicology and Environmental Medicine/Applied Toxicology Branch; 2008.
68. Chonchol M, Nielson C. Hemoglobin levels and coronary artery disease. Am Heart J. 2008;155:494–8.
69. Walker DI, Go Y, Liu K, Pennell K, Jones D, editors. Population screening for biological and environmental properties of the human metabolic phenotype: Implications for personalized medicine. Elsevier, San Diego, CA, USA, 2016.